Magnetic interactions in the cooperative paramagnet $Tb_2Ti_2O_7$

A. Roll [1,2] V. Balédent,[1] J. Robert,[3] J. Ollivier,[4] C. Decorse [5] S. Guitteny,[2] I. Mirebeau [2] and S. Petit[2,*]

[1] *Université Paris-Saclay, CNRS, Laboratoire de Physique des Solides, 91405 Orsay, France*

[2] *Laboratoire Léon Brillouin, CEA, CNRS, Université Paris-Saclay, 91191 Gif sur Yvette, France*

[3] *Université Joseph Fourier, CNRS, Laboratoire Louis Néel, 38042 Grenoble Cedex 9, France*

[4] *Institut Laue Langevin, F-38042 Grenoble, France*

[5] *Université Paris-Saclay, ICMMO, 91405 Orsay, France*

(Received 3 February 2024; accepted 19 August 2024; published 4 October 2024)

For about two decades, $Tb_2Ti_2O_7$ has remained an enigma in condensed matter physics and frustrated magnetism. This material evades long-range order down to temperature as low as 20 mK, and, as in spin ice, its ground state exhibits puzzling diffuse magnetic scattering. To shed light on this issue, we present spin dynamics measurements by inelastic neutron scattering, which we confront with random phase approximation calculations (RPA) to determine exchange couplings capable of reproducing the dispersion of the first excited crystal electric field level. These couplings suggest that $Tb_2Ti_2O_7$ lives at the boundary between several phases, in particular the spin ice and planar antiferromagnetic ones.

DOI: 10.1103/PhysRevResearch.6.043011

I. INTRODUCTION

Geometrically frustrated magnetism is a major research topic in condensed matter physics, as demonstrated by the wealth of new concepts it has generated in recent years [1]. $R_2M_2O_7$ magnets, based on a pyrochlore lattice made from corner sharing tetrahedra, have made a major contribution to this field, exhibiting numerous exotic magnetic ground states such as classical spin ices in $Dy_2Ti_2O_7$ and $Ho_2Ti_2O_7$, ordered spin ices in $Tb_2Sn_2O_7$, ordered antiferromagnetic phase in $Er_2Ti_2O_7$, and Palmer-Chalker ordering in $Er_2Sn_2O_7$ [1–3]. Among most innovative concepts developed in this field, quantum spin ice (QSI) is emblematic [4–7]. This phase of matter evades conventional descriptions, its ground state being a rare example of an intricate wavefunction, formed by a quantum superposition of degenerate spin ice configurations, and where each tetrahedron has two spins pointing toward and two spins pointing outwards its center.

It has long been suspected that $Tb_2Ti_2O_7$ might fall into this category, but no consensus has yet emerged, the physics of this compound remaining an enigma up to date. $Tb_2Ti_2O_7$ was early described as a spin liquid down to 20 mK, characterized by a strong diffuse scattering [8–10] with, notably, the existence of pinch points [11]. Magnetic correlations between longitudinal spin components (along the $\langle 111 \rangle$ cubic direction), bear resemblence with that measured in spin ice (except close to $\mathbf{Q} = 0$), but correlations between transverse spin components, however, show a different pattern, with a "butterfly" motif separated by pinch points, similar to the one expected in the case of isotropic spins coupled by antiferromagnetic interactions.

In most pyrochlore magnets, the first crystal electric field (CEF) excited states are located at high energies, typically above 10 or even 20 meV (200 K), a property that encourages to describe the low temperature properties by focusing on the two states of the ground CEF doublet, using an effective spin 1/2 degree of freedom. Most theoretical approaches [12–15] have therefore considered this approach and neglected the excited levels. It was, however, realized early that the first excited state in $Tb_2Ti_2O_7$ is located at much lower energy, calling this reasoning into question [16,17]. Neutron spectroscopy evidenced that at low temperature, the first excited doublet is actually a collective excitation, a so-called exciton, displaying a clear dispersion around 1.5 meV (15 K), with a significant bandwidth of nearly 1 meV [10,18,19]. This dispersion is due *a priori* to the perturbation of the CEF by magnetic couplings.

In this Letter, we tackle this issue. Our approach combines inelastic neutron scattering and numerical simulations of the spin dynamics based on a model that incorporates not only the ground CEF doublet, but the full CEF scheme. It allows to reproduce the exciton dispersion, hence to determine the magnetic couplings. In this way, it becomes possible to locate $Tb_2Ti_2O_7$ in an enriched mean field phase diagram. Accordingly, this material should be classified as a quantum spin ice, yet at the frontier with planar antiferromagnetic ordered phase.

*Contact author: sylvain.petit@cea.fr

Published by the American Physical Society under the terms of the Creative Commons Attribution 4.0 International license. Further distribution of this work must maintain attribution to the author(s) and the published article's title, journal citation, and DOI.

II. SAMPLE PREPARATION AND EXPERIMENTAL RESULTS

Single crystals were grown by the floating zone method using a four-mirror optical image furnace FZ-T-1400-H-II-PP from Crystal System Inc. with a protocol adapted from

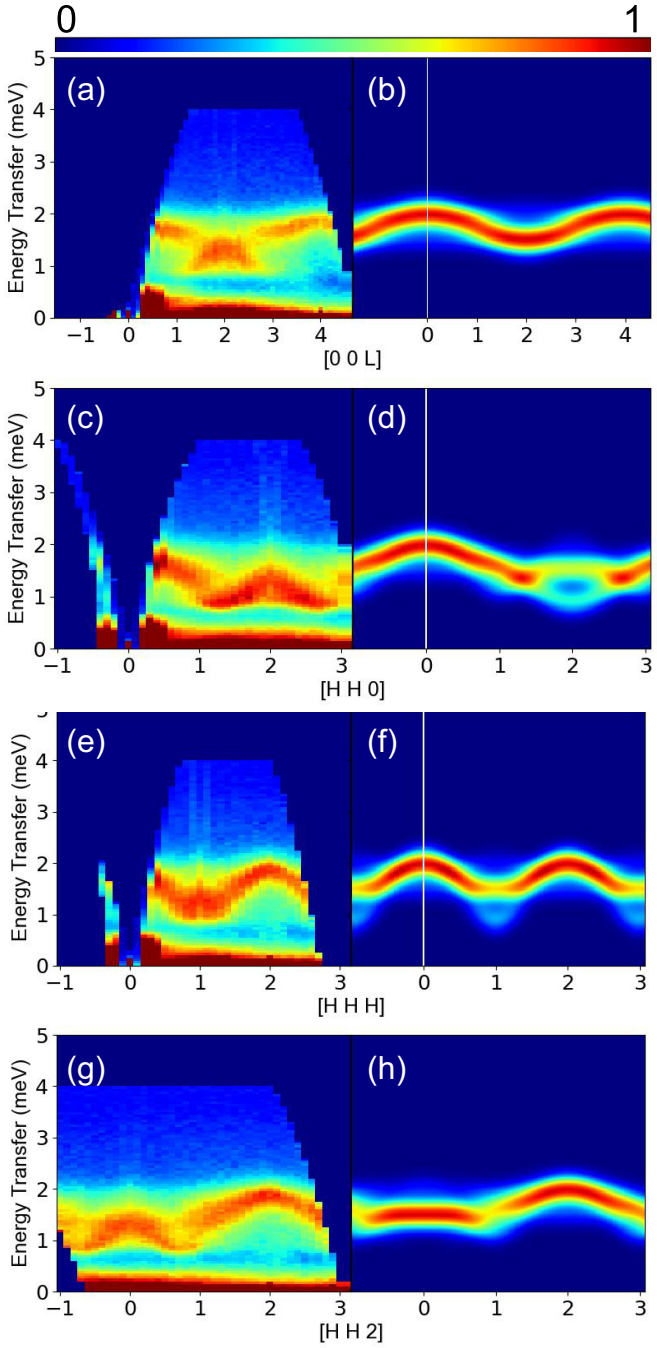

FIG. 1. Comparison between the experimental IN5 time-of-flight $S(Q, \omega)$ intensity taken at 1.5 K (left) with numerical simulations (right) for several directions in reciprocal space. Note that calculations were carried out in the paramagnetic phase of the model at 10 K. The color scale, reported on top of the figure, is in arbitrary units.

Ref. [20]. Inelastic neutron scattering experiments were carried out on the IN5 disk chopper time of flight spectrometer operated by the Institute Laue Langevin (ILL, France). The $Tb_2Ti_2O_7$ single crystal was mounted to have the $(hh0)$-$(00l)$ reciprocal directions in the horizontal scattering plane. Measurements have been performed at 1.5 K (Fig. 1) and 10 K [21]. We used a wavelength $\lambda = 6$ Å, yielding an energy resolution of about 50 μeV. The data were then processed with the HORACE software [22], transforming the recorded time of flight, sample rotation, and scattering angle into energy transfer and Q-wave vectors. The offset of the sample rotation was determined using the position of selected Bragg peak. In all the experiments, the sample was rotated in steps of 0.5 degrees. Slices were taken from the full (Q, ω) dataset to produce maps as a function of energy transfer ω and wave vector Q. The dispersion of the 1.5 meV CEF exciton at 1.5 K is shown on the left column of Fig. 1, along four directions in reciprocal space, namely $(00l)$ (1a), $(hh0)$ (1c), (hhh) (1e), and $(hh2)$ (1g). This dispersion is already visible at 10 K with a narrower bandwith (see [21]). The steep branch stemming from (111) and (220) Bragg positions is the magnetoelastic mode reported in Refs. [18,23].

III. ANALYSIS

To analyze those data, we have chosen a simplified approach, based on a model that takes into account the crystal field as well as interactions between neighboring angular momenta. In a first step, this model is solved at the mean-field level, along the lines of work published in particular in [24]. We then calculated the neutron scattering cross-section using the RPA method, which can be seen as an expansion around the mean-field ground state [21]. We use the model Hamiltonian $\mathcal{H} = \mathcal{H}_{\rm cef} + \mathcal{H}_{\rm mag}$ described hereafter (see also [24]). $\mathcal{H}_{\rm cef}$ is the CEF Hamiltonian, which, owing to the D_{3d} symmetry of the ions writes [25]

$$\mathcal{H}_{\rm cef} = \sum_i \sum_{n,m} \mathcal{B}_m^n \mathcal{O}_{m,i}^n = \mathcal{B}_2^0 \mathcal{O}_2^0 + \mathcal{B}_4^0 \mathcal{O}_{4,i}^0 + \mathcal{B}_4^3 \mathcal{O}_{4,i}^3 + \mathcal{B}_6^0 \mathcal{O}_{6,i}^0 + \mathcal{B}_6^3 \mathcal{O}_{6,i}^3 + \mathcal{B}_6^6 \mathcal{O}_{6,i}^6.$$

Here, the i index runs over the sites of the pyrochlore lattice. The $\mathcal{O}_{m,i}^n$ denote the Stevens operators and the $\mathcal{B}_m^n$ are spectroscopic parameters. A number of studies have been reported in literature proposing different $\mathcal{B}_m^n$ [26–28]. In this work, we use those from [26] and [27] for the sake of generality. The second term $\mathcal{H}_{\rm mag}$ accounts for the bilinear couplings between the total angular moments of the Tb^{3+} ions. In its most general form, taking into account the symmetry of the system, it writes

$$\mathcal{H}_{\rm mag} = \sum_{\langle i,j \rangle} \mathcal{J}^{zz} \mathsf{I}_i^z \mathsf{I}_j^z - \mathcal{J}^{\pm}(\mathsf{I}_i^+ \mathsf{I}_j^- + \mathsf{I}_i^- \mathsf{I}_j^+) + \sum_{\langle i,j \rangle} \mathcal{J}^{\pm\pm}(\gamma_{ij} \mathsf{I}_i^+ \mathsf{I}_j^+ + \gamma_{ij}^* \mathsf{I}_i^- \mathsf{I}_j^-) + \sum_{\langle i,j \rangle} \mathcal{J}^{z\pm}(\xi_{ij} \mathsf{I}_i^z \mathsf{I}_j^+ + \xi_{ij}^* \mathsf{I}_i^z \mathsf{I}_j^-),$$

where (i, j) run over nearest neighbor sites, $\mathcal{J}$ stands for bilinear couplings, ξ_{ij} and γ_{ij} are the bond parameters explicited in Refs. [15,25], and $\mathsf{I}_i^{z,+,-}$ denote the total angular momentum operator of the Tb^{3+} ion at site i, defined in its local frame.

Mean field solutions of this model have been calculated assuming a $\mathbf{q} = 0$ configuration and the obtained magnetic structure have been analyzed using the irreducible representations (IRs) and associated order parameters m_{IR} worked out in [15,21,25]. Those IRs can be divided into two groups. In the first one, the four moments in a tetrahedron lie within the local planes. It includes the antiferromagnet

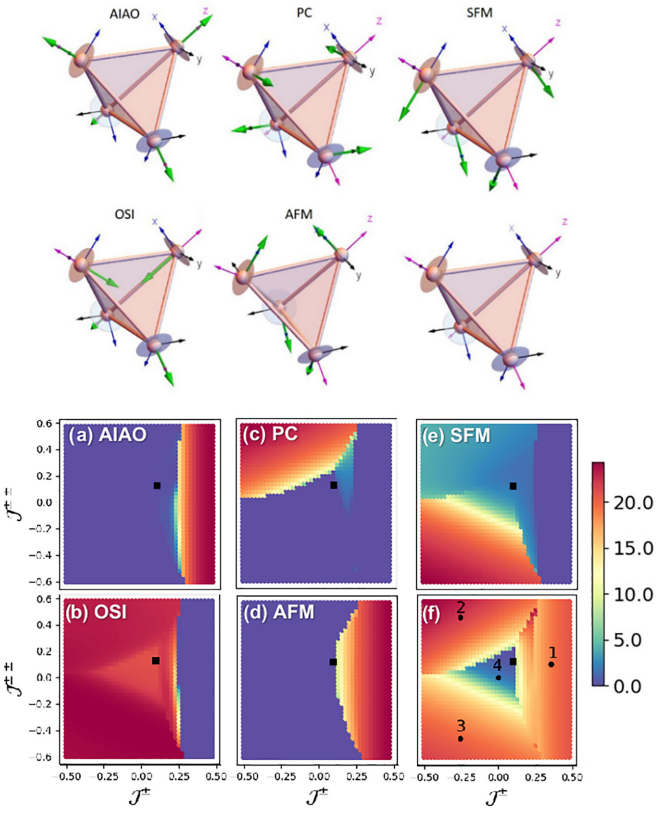

FIG. 2. (Top) Sketches of the various $\mathbf{q} = 0$ IRs entering the description of the mean field magnetic structures. The green arrows represent the magnetic moments. The left bottom corner cartoon shows the bare local axes (blue, black, and magenta for x, y, and z, respectively) while the disks feature the (x, y) local planes. (Bottom) (a)–(e) show the $\alpha, \beta, \gamma, \sigma, \eta$ contributions of the different IR to the mean field solution m, according to the decomposition $m = \alpha\, m_{\rm OSI} + \beta\, m_{\rm AIAO} + \gamma\, m_{\rm AFM} + \sigma\, m_{\rm PC} + \eta\, m_{\rm SFM}$. Calculations are shown for $\mathcal{J}^{z\pm} = 0.03$ K and $\mathcal{J}^{zz} = 0.02$ K. The choice of the former is justified after the fit of the exciton, see Fig. 1. The value of $\mathcal{J}^{zz}$ is chosen according to Ref. [14]. Calculations have been carried out using the $\mathcal{B}_m^n$ reported in [26] but results are essentially unchanged with those from [27] (see [21]). The black square stands for $Tb_2Ti_2O_7$ couplings. (f) represents the superposition of planar IRs contributions $|\gamma| + |\sigma| + |\eta|$ and each black dot stands for a different phase further described in Table I.

(AFM) Γ_5, Palmer-Chalker (PC) Γ_7, and planar vectors of Γ_9 (SFM). In the second group, the moments have finite components along the local z axes only. These are the all-in all-out (AIAO) Γ_3, with moments pointing all-in or all-out of a given tetrahedron, and the remaining basis vectors of Γ_9, called ordered spin ice (OSI), with two moments in and two moments out per tetrahedron. Note that, mean field is in essence not capable of capturing spin ice, the OSI being its counterpart at this level of approximation. The upper part of Fig. 2 gives a sketch of the corresponding magnetic configurations $m_{\rm IR}$ in a tetrahedron. A given mean field solution m is a superposition of the different order parameters: $m = \alpha\, m_{\rm OSI} + \beta\, m_{\rm AIAO} + \gamma\, m_{\rm AFM} + \sigma\, m_{\rm PC} + \eta\, m_{\rm SFM}$.
Figures 2(a)–2(e) (bottom) display the contributions $\alpha, \beta, \gamma, \sigma$, and η for $\mathcal{J}^{\pm\pm}$ vs $\mathcal{J}^{\pm}$ and $\mathcal{J}^{z\pm} = 0.03$ K, $\mathcal{J}^{zz} = 0.02$ K, the latter value being chosen according to the study presented in Ref. [14]. We observe that PC and SFM are associated with OSI and favored by $\mathcal{J}^{\pm\pm}$ and $\mathcal{J}^{z\pm}$, whereas AFM, favored by $\mathcal{J}^{\pm}$ goes along with AIAO. Furthermore, in a limited region close to $\mathcal{J}^{\pm} \approx 0.1$ K, AFM is dominant with small PC and SFM contributions. Beyond $\mathcal{J}^{\pm} \approx 0.25$ K, the latter two contributions disappear and the configuration becomes AFM+AIAO. Entanglement between z and planar components is a very general trend throughout the phase diagram. We argue that this results from $\mathcal{H}_{\rm cef}$ in the model, which, unlike spin 1/2 approaches, allows virtual crystal field transitions that couple the z and planar components of the magnetic moments [16,29]. To better figure out the deviation out of OSI or AIAO configurations, where the moments are purely along the z axes, Fig. 2(f) shows the sum of the planar AFM, PC, and SFM contributions $|\gamma| + |\sigma| + |\eta|$. Table I also gives those normalized contributions for several points shown in Fig. 2(f) (black dots). Figure 3 is a 3D plot showing the same quantity as a function of $\mathcal{J}^{\pm}$, $\mathcal{J}^{\pm\pm}$, and $\mathcal{J}^{z\pm}$. Figure 2(f) can then be seen as a 2D slice at $\mathcal{J}^{z\pm} = 0.03$ of Fig. 3.

TABLE I. Contributions of the different IR to the mean field solution, according to the decomposition $m = \alpha\, m_{\rm OSI} + \beta\, m_{\rm AIAO} + \gamma\, m_{\rm AFM} + \sigma\, m_{\rm PC} + \eta\, m_{\rm SFM}$. Coefficients are normalized to $\alpha^2 + \beta^2 + \gamma^2 + \sigma^2 + \eta^2$. The quantity $\rho = (\gamma^2 + \sigma^2 + \eta^2)/(\alpha^2 + \beta^2)$ features the planar character of m. Positions are labeled by dots in Fig. 2(f). $\mathcal{B}_m^n$ are taken from [26].

Position	ρ planar/z	$\tilde{\alpha}$ OSI	$\tilde{\beta}$ AIAO	$\tilde{\gamma}$ AFM	$\tilde{\sigma}$ PC	$\tilde{\eta}$ SFM
1	1.00	0	0.699	0.715	0	0
2	0.79	0.747	0	0	0.656	0.108
3	0.79	0.747	0	0	0	0.664
4	0.03	0.985	0	0	0	0.174
TTO	0.11	0.950	0.011	0.304	0	0.081

In order to determine the magnetic couplings and thus locate $Tb_2Ti_2O_7$ in this phase diagram, the dispersion of the exciton was calculated within the framework of the random phase approximation (RPA). Calculations were carried out in the paramagnetic regime at 10 K to match the experimental situation. The fit quality is evaluated using a criterion based on the difference in the energy position of the intensity maximum between measurement and calculation, at different Q values over the studied range. The three-dimensional parameter space ($\mathcal{J}^{\pm}$, $\mathcal{J}^{\pm\pm}$, $\mathcal{J}^{z\pm}$) was systematically explored, fixing $\mathcal{J}^{zz}$ to 0.02 K, with the aim of reproducing the experimental dispersion of the first excited CEF state. The right column of Fig. 1 shows the simulations which yield the best agreement vs experiments. The values of the couplings are given in Table II. Slight modifications around those optimized values do not significantly affect the dispersion, allowing to estimate a range of uncertainty for each refined parameter, as reported in Table II. Calculations match well the experiment in all investigated directions of the reciprocal space, with a small caveat regarding the dispersion along the $(00l)$ direction. Note that close to Brillouin zone centers, the acoustic phonon might influence the first CEF excited state at the crossing point, owing to magnetoelastic coupling [10,18,23,30], a physical ingredient not taken into account in the present model. Precise

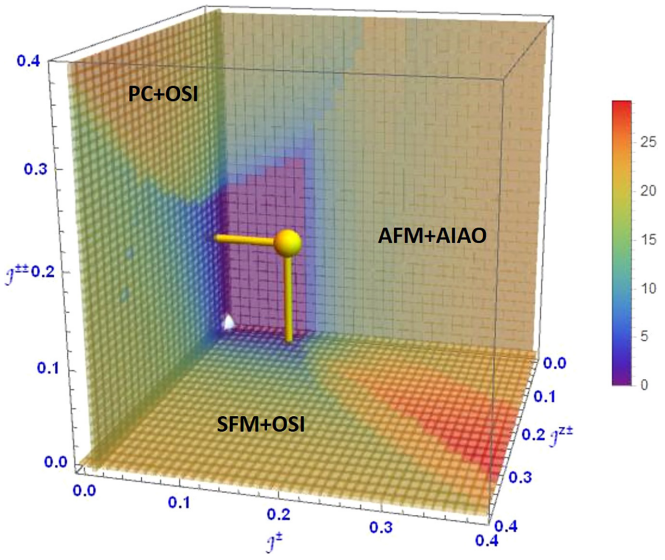

FIG. 3. Magnetic phase diagram obtained from mean field solution of the model Hamiltonian $\mathcal{H} = \mathcal{H}_{\rm cef} + \mathcal{H}_{\rm mag}$ (see text). The color scale represents the sum of the contributions from the planar IRs: antiferromagnet (AFM), Palmer-Chalker (PC), and splayed ferromagnet (SFM). The yellow sphere shows the location of $Tb_2Ti_2O_7$; the white one, in the corner, stands for pure spin ice phase. $\mathcal{B}_m^n$ are taken from [26]. Calculations based on [27] can be found in the Supplemental Material [21].

numerical values of the magnetic couplings may depend on the choice of the $\mathcal{B}_m^n$, but conclusions, however, remain unchanged whether using [26] or [27] (see [21]).

With these values and according to the phase diagram of Fig. 2, $Tb_2Ti_2O_7$ is located at the frontier between the OSI and the AIAO + AFM phase. As shown in Table I, it is described by OSI as primary IR, but also contains AFM and SFM, owing to non-negligable weight γ and η. This projection can thus explain the fluctuating character of $Tb_2Ti_2O_7$ ground state. Furthermore, such a proximity with ordered phases suggests that it might be possible, with external perturbations such as pressure or magnetic field, to drive $Tb_2Ti_2O_7$ toward an ordered magnetic phase, as observed experimentally [31–33]. Finally, the non-negligable γ AFM weight (cf. I) sheds light on the fact that the diffuse scattering between transverse components of the magnetic moments is reminiscent of expectations in the case of a frustrated (isotropic) antiferromagnet [9].

TABLE II. Magnetic couplings (in K) corresponding to the best fit to the experimental dispersion, and obtained from RPA calculations (see Fig. 1). The uncertainty range is given in the last column.

Interaction	Value in Fig. 1	Uncertainty range
$\mathcal{J}^{\pm}$	0.125	[0.1:0.125]
$\mathcal{J}^{\pm\pm}$	0.1	[0.1:0.125]
$\mathcal{J}^{z\pm}$	0.03	[0:0.05]
$\mathcal{J}^{zz}$	0.02	[−0.003:0.1]

IV. DISCUSSION AND CONCLUSION

So far, a number of studies have considered a model formally identical to $\mathcal{H}_{\rm mag}$, written for the pseudospin 1/2 degree of freedom spanning the CEF ground doublet states [12–14,25,34]. For non-Kramers ions such as Tb^{3+}, projections of J^x and J^y onto the CEF ground doublet are zero, and J^z identifies with the z component of the pseudospin. As a result, $\mathcal{J}^{zz}$ is left as the only coupling of purely magnetic origin in pseudospin 1/2 approaches. As it comprises the complexity of the CEF scheme, the present study allows to envisage the role of magnetic couplings beyond $\mathcal{J}^{zz}$. Here we show that indeed the magnetic couplings $\mathcal{J}^{\pm}$, $\mathcal{J}^{\pm\pm}$, and $\mathcal{J}^{z\pm}$ are relevant.

Furthermore, as explained in Ref. [13], the x and y components of the pseudospin represent different combinations of the quadrupolar moments in the case of non-Kramers ions. Ordered states for those components should then be understood as quadrupolar states. Reference [14] especially places $Tb_2Ti_2O_7$ in one of those long range ordered quadrupolar phases, yet close to the border with the QSI area. This conclusion raises some doubts because, in such a scenario, the magnetic moment at each site is zero, which cannot account for the existence of the diffuse magnetic scattering reported in $Tb_2Ti_2O_7$ long ago [9,35]. This physics is not taken into account in the present work, since $\mathcal{H}$ does not consider quadrupole-quadrupole terms. In our view, the two approaches are, however, complementary, and need to be combined in a common model, which remains to be worked out. Indeed, a last experimental feature concerns the low-energy sector of the spin dynamics, below 0.3 meV. Some time ago, by means of polarized and unpolarized inelastic neutron scattering experiments performed on single crystal and powder, Refs. [10,14] reported the existence of another dispersing mode in this energy range. Due to the non-Kramers nature of Tb^{3+}, a long series of works have shown that magnetic dipole-dipole interactions are not sufficient to understand the strong spectral weight of this mode, a feature that is, however, amenable by introducing quadrupole-quadrupole interactions [10,19,36,37].

In conclusion, the analysis of the exciton dispersion locates $Tb_2Ti_2O_7$ at the border between OSI and AFM+AIAO in a mean field phase diagram. This result suggests that $Tb_2Ti_2O_7$ is a convincing candidate for a quantum spin liquid state lying very close to an antiferromagnetic phase. This would explain its fluctuating behavior and deep differences with canonical spin ice. Quadrupolar interactions are also very likely at play and their influence will be considered in a separate publication.

ACKNOWLEDGMENTS

This work was financially supported by ANR COCOM 20-CE30-0029 and FRAGMENT 19-CE30-0040. We acknowledge the MORPHEUS platform at the Laboratoire de Physique des Solides and the ORIENTEXPRESS beamline at ILL for sample alignment. The authors thank Q. Faure, A. Gukassov, F. Damay, and P. McClarty for useful discussions.

[1] *Introduction to Frustrated Magnetism*, edited by C. Lacroix, P. Mendels, and F. Mila (Springer-Verlag, Berlin, 2011).

[2] M. J. P. Gingras and P. A. McClarty, Quantum spin ice: A search for gapless quantum spin liquids in pyrochlore magnets, Rep. Prog. Phys. **77**, 056501 (2014).

[3] J. S. Gardner, M. J. P. Gingras, and J. E. Greedan, Magnetic pyrochlore oxides, Rev. Mod. Phys. **82**, 53 (2010).

[4] C. L. Henley, The "coulomb phase" in frustrated systems, Annu. Rev. Condens. Matter Phys. **1**, 179 (2010).

[5] M. Hermele, M. P. A. Fisher, and L. Balents, Pyrochlore photons: The $U(1)$ spin liquid in a $S = 1/2$ three-dimensional frustrated magnet, Phys. Rev. B **69**, 064404 (2004).

[6] N. Shannon, O. Sikora, F. Pollmann, K. Penc, and P. Fulde, Quantum ice: A quantum Monte Carlo study, Phys. Rev. Lett. **108**, 067204 (2012).

[7] O. Benton, O. Sikora, and N. Shannon, Seeing the light: Experimental signatures of emergent electromagnetism in a quantum spin ice, Phys. Rev. B **86**, 075154 (2012).

[8] J. S. Gardner, S. R. Dunsiger, B. D. Gaulin, M. J. P. Gingras, J. E. Greedan, R. F. Kiefl, M. D. Lumsden, W. A. MacFarlane, N. P. Raju, J. E. Sonier, I. Swainson, and Z. Tun, Cooperative paramagnetism in the geometrically frustrated pyrochlore antiferromagnet $Tb_2Ti_2O_7$, Phys. Rev. Lett. **82**, 1012 (1999).

[9] T. Fennell, M. Kenzelmann, B. Roessli, M. K. Haas, and R. J. Cava, Power-law spin correlations in the pyrochlore antiferromagnet $Tb_2Ti_2O_7$, Phys. Rev. Lett. **109**, 017201 (2012).

[10] S. Guitteny, J. Robert, P. Bonville, J. Ollivier, C. Decorse, P. Steffens, M. Boehm, H. Mutka, I. Mirebeau, and S. Petit, Anisotropic propagating excitations and quadrupolar effects in $Tb_2Ti_2O_7$, Phys. Rev. Lett. **111**, 087201 (2013).

[11] T. Fennell, P. P. Deen, A. R. Wildes, K. Schmalzl, D. Prabhakaran, A. T. Boothroyd, R. J. Aldus, D. F. McMorrow, and S. T. Bramwell, Magnetic coulomb phase in the spin ice $Ho_2Ti_2O_7$, Science **326**, 415 (2009).

[12] L. Savary and L. Balents, Coulombic quantum liquids in spin-1/2 pyrochlores, Phys. Rev. Lett. **108**, 037202 (2012).

[13] S. Lee, S. Onoda, and L. Balents, Generic quantum spin ice, Phys. Rev. B **86**, 104412 (2012).

[14] H. Takatsu, S. Onoda, S. Kittaka, A. Kasahara, Y. Kono, T. Sakakibara, Y. Kato, B. Fåk, J. Ollivier, J. W. Lynn *et al.*, Quadrupole order in the frustrated pyrochlore $Tb_{2+x}Ti_{2-x}O_{7+y}$, Phys. Rev. Lett. **116**, 217201 (2016).

[15] H. Yan, O. Benton, L. Jaubert, and N. Shannon, Theory of multiple-phase competition in pyrochlore magnets with anisotropic exchange with application to $Yb_2Ti_2O_7$, $Er_2Ti_2O_7$, and $Er_2Sn_2O_7$, Phys. Rev. B **95**, 094422 (2017).

[16] Y.-J. Kao, M. Enjalran, A. D. Maestro, H. R. Molavian, and M. J. P. Gingras, Understanding paramagnetic spin correlations in the spin-liquid pyrochlore $Tb_2Ti_2O_7$, Phys. Rev. B **68**, 172407 (2003).

[17] H. R. Molavian, M. J. P. Gingras, and B. Canals, Dynamically induced frustration as a route to a quantum spin ice state in $Tb_2Ti_2O_7$ via virtual crystal field excitations and quantum many-body effects, Phys. Rev. Lett. **98**, 157204 (2007).

[18] T. Fennell, M. Kenzelmann, B. Roessli, H. Mutka, J. Ollivier, M. Ruminy, U. Stuhr, O. Zaharko, L. Bovo, A. Cervellino *et al.*, Magnetoelastic excitations in the pyrochlore spin liquid $Tb_2Ti_2O_7$, Phys. Rev. Lett. **112**, 017203 (2014).

[19] S. Petit, P. Bonville, I. Mirebeau, H. Mutka, and J. Robert, Spin dynamics in the ordered spin ice $Tb_2Sn_2O_7$, Phys. Rev. B **85**, 054428 (2012).

[20] J. S. Gardner, B. D. Gaulin, and D. M. Paul, Single crystal growth by the floating-zone method of a geometrically frustrated pyrochlore antiferromagnet, $Tb_2Ti_2O_7$, J. Cryst. Growth **191**, 740 (1998).

[21] See Supplemental Material at http://link.aps.org/supplemental/10.1103/PhysRevResearch.6.043011 for additional information regarding INS data and calculations, especially simulations obtained for three different sets of crystal field parameters reported in literature.

[22] R. A. Ewings, A. Buts, M. D. Le, J. V. Duijn, I. Bustinduy, and T. G. Perring, Horace: Software for the analysis of data from single crystal spectroscopy experiments at time-of-flight neutron instruments, Nucl. Instrum. Methods Phys Res. Sect. A **834**, 132 (2016).

[23] M. Ruminy, S. Guitteny, J. Robert, L.-P. Regnault, M. Boehm, P. Steffens, H. Mutka, J. Ollivier, U. Stuhr, J. S. White *et al.*, Magnetoelastic excitation spectrum in the rare-earth pyrochlore $Tb_2Ti_2O_7$, Phys. Rev. B **99**, 224431 (2019).

[24] A. M. Hallas, W. Jin, J. Gaudet, E. M. Tonita, D. Pomaranski, C. R. C. Buhariwalla, M. Tachibana, N. P. Butch, S. Calder, M. B. Stone *et al.*, Intertwined magnetic dipolar and electric quadrupolar correlations in the pyrochlore $Tb_2Ge_2O_7$, arXiv:2009.05036.

[25] J. G. Rau and M. J. P. Gingras, Frustrated quantum rare-earth pyrochlores, Annu. Rev. Condens. Matter Phys. **10**, 357 (2019).

[26] I. Mirebeau, P. Bonville, and M. Hennion, Magnetic excitations in $Tb_2Sn_2O_7$ and $Tb_2Ti_2O_7$ as measured by inelastic neutron scattering, Phys. Rev. B **76**, 184436 (2007).

[27] J. Zhang, K. Fritsch, Z. Hao, B. V. Bagheri, M. J. P. Gingras, G. E. Granroth, P. Jiramongkolchai, R. J. Cava, and B. D. Gaulin, Neutron spectroscopic study of crystal field excitations in $Tb_2Ti_2O_7$ and $Tb_2Sn_2O_7$, Phys. Rev. B **89**, 134410 (2014).

[28] A. J. Princep, H. C. Walker, D. T. Adroja, D. Prabhakaran, and A. T. Boothroyd, Crystal field states of Tb^{3+} in the pyrochlore spin liquid $Tb_2Ti_2O_7$ from neutron spectroscopy, Phys. Rev. B **91**, 224430 (2015).

[29] J. G. Rau, S. Petit, and M. J. P. Gingras, Order by virtual crystal field fluctuations in pyrochlore xy antiferromagnets, Phys. Rev. B **93**, 184408 (2016).

[30] A. A. Turrini, M. Ruminy, F. Bourdarot, U. Stuhr, J. S. White, G. Tucker, M. Skoulatos, M. Núñez-Valdez, and T. Fennell, Magnetic-field control of magnetoelastic coupling in the rare-earth pyrochlore $Tb_2Ti_2O_7$, Phys. Rev. B **104**, 224403 (2021).

[31] K. C. Rule, J. P. C. Ruff, B. D. Gaulin, S. R. Dunsiger, J. S. Gardner, J. P. Clancy, M. J. Lewis, H. A. Dabkowska, I. Mirebeau, P. Manuel *et al.*, Field-induced order and spin waves in the pyrochlore antiferromagnet $Tb_2Ti_2O_7$, Phys. Rev. Lett. **96**, 177201 (2006).

[32] J. P. C. Ruff, B. D. Gaulin, J. P. Castellan, K. C. Rule, J. P. Clancy, J. Rodriguez, and H. A. Dabkowska, Structural fluctuations in the spin-liquid state of $Tb_2Ti_2O_7$, Phys. Rev. Lett. **99**, 237202 (2007).

[33] I. Mirebeau, I. N. Goncharenko, P. Cadavez-Peres, S. T. Bramwell, M. J. P. Gingras, and J. S. Gardner, Pressure-induced crystallization of a spin liquid, Nature (London) **420**, 54 (2002).

[34] K. A. Ross, L. Savary, B. D. Gaulin, and L. Balents, Quantum excitations in quantum spin ice, Phys. Rev. X **1**, 021002 (2011).

[35] J. S. Gardner, B. D. Gaulin, A. J. Berlinsky, P. Waldron, S. R. Dunsiger, N. P. Raju, and J. E. Greedan, Neutron scattering studies of the cooperative paramagnet pyrochlore $Tb_2Ti_2O_7$, Phys. Rev. B **64**, 224416 (2001).

[36] S. Petit, P. Bonville, J. Robert, C. Decorse, and I. Mirebeau, Spin liquid correlations, anisotropic exchange, and symmetry breaking in $Tb_2Ti_2O_7$, Phys. Rev. B **86**, 174403 (2012).

[37] P. Bonville, I. Mirebeau, A. Gukasov, S. Petit, and J. Robert, Tetragonal distortion yielding a two-singlet spin liquid in pyrochlore $Tb_2Ti_2O_7$, Phys. Rev. B **84**, 184409 (2011).